9

Compact Heat Exchange Reformer Used for High Temperature Fuel Cell Systems

Huisheng Zhang, Shilie Weng and Ming Su
Shanghai Jiao Tong University
China

1. Introduction

High temperature fuel cell systems are an attractive emerging technology for stationary power generation, especially for the distributed generation [1]. Today, there are mainly two types of high temperature fuel cell systems, including the molten carbonate fuel cell (MCFC) and solid oxide fuel cell (SOFC), which are generally operated at high temperatures ranging from 823K to 1273K. Several advantages of this setup are listed in the references [2]. The main advantages of both fuel cells are related to what could be done with the waste heat and how they can be used to reform fuels, provide heat, and drive engines. Therefore, high temperature fuel cell systems can never be simply considered as fuel cells; instead, they must always be thought of as an integral part of a complete fuel processing and heat generating system [2].

Steam reforming is a well-established industrial fuel process for producing hydrogen or synthetic gas from natural gas, other hydrocarbon fuels, and alcohols [3]. In the high temperature fuel cell systems, the pre-reformer is usually needed for fuel processing. Due to the high endothermic reaction, a great amount of heat must be provided from the outside, such as waste heat from the fuel cell, catalyst combustion, etc.

High temperature heat exchangers are widely used in the high temperature fuel cell/gas turbine system, closed cycle gas turbine system, high temperature gas cooled reactors, and other thermal power systems. It is an effective method of improving the whole system efficiency [4]. Compact heat exchangers are generally characterized by extended surfaces with large surface area/volume ratios that are often configured in either plate-fin or tube-fin arrangements [5]. In a plate-fin exchanger, many augmented surface types are used: plain-fins, wavy fins, offset strip fins, perforated fins, pin fins, and louvered fins. Offset strip fins, which have a high degree of surface compactness and feasible manufacturing, are very widely applied.

In general, the high temperature heat exchanger is used to preheat the air or fuel, while the pre-reformer is used to produce hydrogen rich fuel from methane or other hydrocarbons. Fig. 1 shows one of the fuel cell systems, which consists of a direct internal reforming solid oxide fuel cell (DIR-SOFC), a high temperature heat exchanger (HTHE), a low temperature heat exchanger (LTHE), a pre-reformer, a gas turbine, a generator, etc. In order to simplify the system, reduce the cost, and improve the fuel cell system's efficiency, it is suggested that

a compact heat exchange reformer replace the heat exchanger and the pre-reformer. The new fuel cell system is illustrated in Fig. 2. The offset strip fin heat exchanger and pre-reformer are combined into the heat exchange reformer. In this device with the counter-flow type, the high temperature waste gas from the fuel cell flows in the hot passage, and the fuel flows in the cold passage. In particular, the Ni catalyst is coated on the fuel passage surface [6, 7]. When the fuel flows along the passage, the endothermic steam reforming reaction will take place using the heat transferring from the hot side.

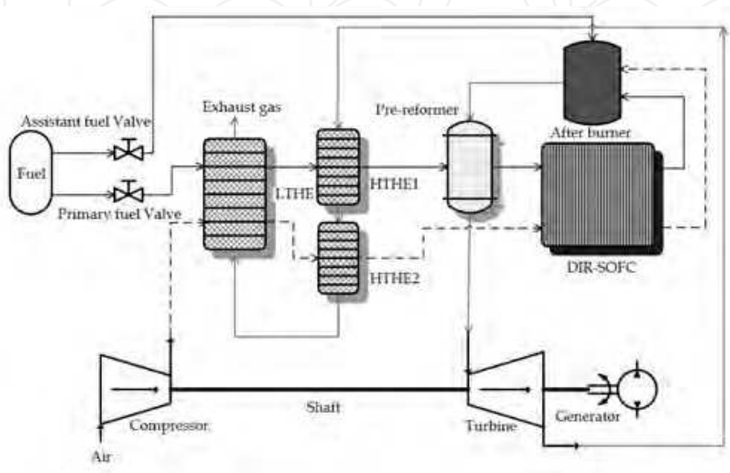

Fig. 1. Schematic view of the traditional SOFC/GT hybrid system.

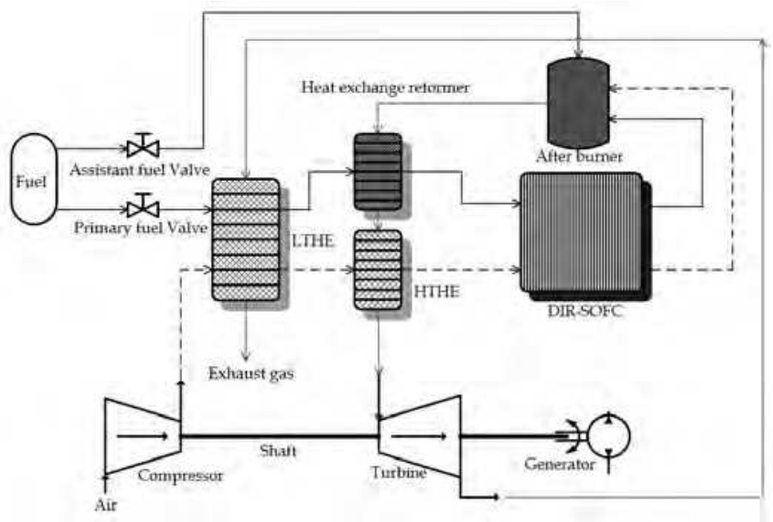

Fig. 2. Schematic view of the SOFC/GT hybrid system with novel concept heat exchange reformer.

Several kinds of compact heat exchange reformers have been investigated and designed in the past. In 2001, Kawasaki Heavy Industries in Japan developed a plate-fin heat-exchange reformer with highly dispersed catalyst [8]. A planar micro-channel concept was proposed by Pacific Northwest National Laboratories (PNNL), but this kind of micro-channel device is oriented toward the low to medium power range (20-500W) for man-portable applications

[9, 10]. A novel micro fuel processor for PEMFCs with heat generation by catalytic combustion was developed and characterized in South Korea [11-13].

All these previous works were mainly developed based on experiments, but the steady state and dynamic performance simulations have not been investigated in detail. The heat supplied for the methane steam reforming reaction has different sources, such as catalytic combustion [11, 12] and auto-thermal methane reforming reactions [10]. The purposes are mainly for the portable devices [9, 10] or the low temperature fuel cells [11-13]. Here, the waste heat from the high temperature fuel cell systems will be used as the heat resource in the compact heat exchange reformer for the steam reforming reaction.

This chapter aims to: design a compact heat exchange reformer for the high temperature fuel cell systems; develop a real time simulation model using the volume-resistance characteristic modeling technique; study the steady state distribution characteristics by considering local fluid properties such as pressure, velocity, density, heat capacity, thermal conductivity, dynamic viscosity, etc; discuss some factors that will affect the performance of the reformer during steady state operation under the same operating condition; and finally, investigate dynamic behavior under different input parameters including step-change conditions.

2. Description of heat exchange reformer

2.1 Configuration

The configuration of the heat exchange reformer is similar to the compact heat exchanger. The only difference is that the catalyst is coated in the cold passage to make steam reforming reactions take place.

As shown in Fig. 3, the configuration of the offset strip fin heat exchanger is adopted here. The fin surface is broken into a number of smaller sections. Generally, each type of fin is characterized by its width *X*, height *Y*, thickness *t*, and length of the offset strip fin *l*. The detailed configuration can also be found in other references for the heat exchanger [14-18].

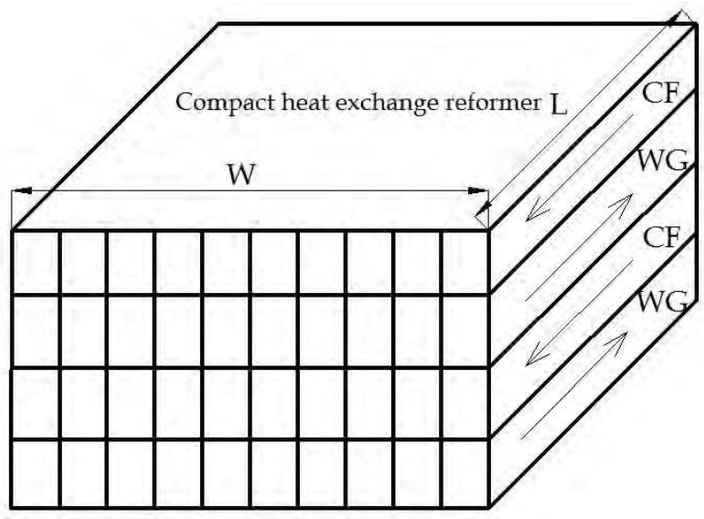

(a)

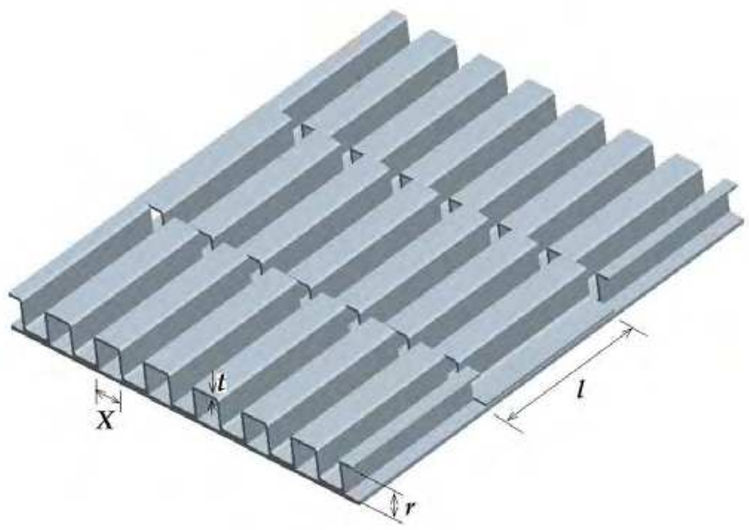

(b)

Fig. 3. Flow (a) and fin structure (b) diagram of heat exchange reformer.

Taking the hot passage as an example, the calculations for individual geometry variables are listed as following:

$$\text{Passage number: } n_{\mathrm{h}} = W/\left(X_{\mathrm{h}} + t_{\mathrm{h}}\right) \tag{1}$$

$$\text{Offset strip number: } n_{\mathrm{h}l} = L/l_{\mathrm{h}} \tag{2}$$

$$\text{Cross area of flow passage: } A_{\mathrm{h}} = n_{\mathrm{h}} X_{\mathrm{h}} Y_{\mathrm{h}} \tag{3}$$

$$\text{Heat transfer surface of flow passage: } S_{\mathrm{h}} = 2n_{\mathrm{h}}\left(X_{\mathrm{h}} + Y_{\mathrm{h}}\right)L + n_{\mathrm{h}l} n_{\mathrm{h}}\left(X_{\mathrm{h}} + Y_{\mathrm{h}} + t_{\mathrm{h}}\right)t_{\mathrm{h}} \tag{4}$$

$$\text{Wet perimeter: } U_{\mathrm{h}} = 4S_{\mathrm{h}}/L \tag{5}$$

$$\text{Hydraulic diameter: } D_{\mathrm{h}} = 4A_{\mathrm{h}} / U_{\mathrm{h}} \tag{6}$$

2.2 Passage fin efficiency

The passage fin efficiency η_0 is given by Rosehnow et al. [18] as

$$\eta_0 = 1 - \frac{S_{\mathrm{f}}}{S}\left(1 - \eta_{\mathrm{f}}\right) \tag{7}$$

where the secondary heat transfer area of a stream S_{f} for the hot passage equals S_{h}. The total area of the heat exchanger S is calculated by the sum of the primary heat transfer surface and the secondary heat transfer area of a stream.

According to Rosehnow et al. [15, 18], the fin efficiency for the offset strip fin with a rectangular section can be approximated by:

$$\eta_{\mathrm{f,h}} = \frac{\tanh(m_{\mathrm{h}} k_{\mathrm{h}})}{m_{\mathrm{h}} k_{\mathrm{h}}} \tag{8}$$

where,

$$m_{\mathrm{h}} = \sqrt{\frac{\alpha_{\mathrm{h}} U_{\mathrm{h}}}{\lambda_{\mathrm{h}} f_{\mathrm{h}}}}\ ,\ k_{\mathrm{h}} = Y_{\mathrm{h}}/2 - t_{\mathrm{h}}\ .$$

Finally, the fin efficiency can be simplified by:

$$\eta_{0,\mathrm{h}} = 1 - \frac{Y_{\mathrm{h}}}{X_{\mathrm{h}} + Y_{\mathrm{h}}}(1 - \eta_{\mathrm{f,h}}) \tag{9}$$

The fin efficiency is mainly influenced by the material, configuration of the fin, and the heat transfer coefficient between the fin and the flow.

2.3 Pressure loss

The frictional pressure loss across an offset strip fin passage and at any associated entry, exit, and turning loss [15], can be expressed by:

$$\Delta P = 4f\left(\frac{L}{D_h}\right)\left(\frac{G_m{}^2}{2\rho}\right) + K\left(\frac{G_m{}^2}{2\rho}\right) \tag{10}$$

where, $G_m = \rho u$.

Here, turning losses are neglected, so the pressure loss per unit length can be expressed by:

$$\frac{\Delta P}{L} = \frac{U}{A}\left(\frac{1}{2} f \rho u^2\right) \tag{11}$$

Let the friction resistance $\sigma = \frac{1}{2} f \rho u^2$,

Then,

$$\frac{\mathrm{d}P}{\mathrm{d}x} = \frac{U\sigma}{A} \tag{12}$$

The fanning friction factor f has been developed by many authors. Basing on the data of Kays & London [14], Manglik & Bergles [17] recommend:

$$\begin{aligned} f &= 9.6243\,\mathrm{Re}^{-0.7422}\,\alpha^{-0.1856}\delta^{0.3053}\gamma^{-0.2659} \\ &\times\left[\,1+7.669\times10^{-8}\,\mathrm{Re}^{4.429}\,\alpha^{0.920}\delta^{3.767}\gamma^{0.236}\,\right]^{0.1} \end{aligned} \tag{13}$$

2.4 Heat transfer coefficient

Generally, the heat transfer coefficient α is related to the Colburn factor [15, 17, 18] and is expressed as:

$$\alpha = JG_m c_p \,\mathrm{Pr}^{-2/3} \tag{14}$$

where the Colburn factor $J = St\,\mathrm{Pr}^{2/3}$ and the Prandtl number $\mathrm{Pr} = \mu c_p / \lambda$.

The correlation developed by Manglik & Bergles [17] from the data of Kays & London [14] reads:

$$J = 0.6522\,\mathrm{Re}^{-0.5403}\,\alpha^{-0.1541}\delta^{0.1499}\gamma^{-0.0678} \times \left[1+5.269\times10^{-5}\,\mathrm{Re}^{1.340}\,\alpha^{0.504}\delta^{0.456}\gamma^{-1.055}\right]^{0.1} \tag{15}$$

2.5 Steam reforming

In the cold fuel passage, the steam reforming reaction (I), water gas shift reaction (II), and CO_2 direct reforming reactions of methane (III) are carried out over a Ni catalyst coat on the passage surface at sufficiently high temperatures, typically above 773K.

Kinetic rate equations for the reactions (I-III) are adopted from Xu and Froment [19]. The three kinetic rate equations are listed in Table 1 as well.

(I)	$CH_4 + H_2O \Leftrightarrow CO + 3H_2$	$R_{(I)} = \frac{k_1}{p_{H_2}^{2.5}}\left(p_{CH_4}p_{H_2O} - \frac{p_{H_2}^3 p_{CO}}{K_{e1}}\right) * \frac{1}{DEN^2}$	(16)
(II)	$CO + H_2O \Leftrightarrow CO_2 + H_2$	$R_{(II)} = \frac{k_2}{p_{H_2}}\left(p_{CO}p_{H_2O} - \frac{p_{H_2}p_{CO_2}}{K_{e2}}\right) * \frac{1}{DEN^2}$	(17)
(III)	$CH_4 + 2H_2O \Leftrightarrow CO_2 + 4H_2$	$R_{(III)} = \frac{k_3}{p_{H_2}^{3.5}}\left(p_{CH_4}p_{H_2O}^2 - \frac{p_{H_2}^4 p_{CO_2}}{K_{e3}}\right) * \frac{1}{DEN^2}$	(18)

Table 1. Reaction and its rate in the heat exchange reformer (Xu and Froment, [19]).

The enthalpy changes of chemical reactions are calculated according to Smit et.al [20].

$$\Delta H_{(I)} = \Delta H_{(I)}^0 - 16373.61 + R\left(7.951T_c - 4.354e-3T_c^2 + 0.7213e-6T_c^3 - 0.097e5/T_c\right) \tag{19}$$

$$\Delta H_{(II)} = \Delta H_{(II)}^0 - 7756.56 + R\left(1.86T_c - 0.27e-3T_c^2 + 1.164e5/T_c\right) \tag{20}$$

$$\Delta H_{(III)} = \Delta H_{(III)}^0 - 26125.07 + R\left(10.657T_c - 4.624e-3T_c^2 + 0.7213e-6T_c^3 + 1.067e5/T_c\right) \tag{21}$$

3. Mathematic model of heat exchange reformer

To simplify the complexity of the mathematical model, some assumptions [4, 21] adopted in the theoretic analysis are presented as follows:

1. The heat exchange reformer is adiabatic to the surrounding;

2. The viscosity dissipation effects are neglected;
3. The parameters are considered to be uniform over a cross-section, one dimensional flow along the passage, without inside circumfluence;
4. For the horizontal fluid, the effect of height change can be omitted.

In the cold fuel passage, the chemical species are CH_4, H_2, CO, CO_2, and H_2O. Species mass balances in the cold fuel passage are considered.

$$\frac{\partial C_{c,i}}{\partial t} = -u_c \frac{\partial C_{c,i}}{\partial x} + \sum_{k\in\{(I),(II),(III)\}} v_{i,k} R_k \frac{1}{Y_c} \quad i \in \{CH_4, H_2, CO, CO_2, H_2O\} \tag{22}$$

The mass, momentum, and energy conservation equations for the hot passage and cold passage are established in Table 2 and Table 3, respectively. In the hot passage, the heat transfer to the solid structure is considered. Due to the very thin catalyst coat, the enthalpy changes of the reactions (I-III) are also considered in the cold passage, in addition to the heat transferred from the solid structure.

Mass conservation equation
$$\frac{\partial \rho_h}{\partial t} = -\frac{\partial(\rho_h u_h)}{\partial x} \tag{23}$$
Momentum conservation equation
$$\frac{\partial(\rho_h u_h)}{\partial t} = -\frac{\partial(\rho_h u_h^2)}{\partial x} - \frac{\partial P_h}{\partial x} - \frac{U_h \sigma_h}{A_h} \tag{24}$$
Energy conservation equation
$$\frac{\partial T_h}{\partial t} = -u_h \frac{\partial T_h}{\partial x} - \frac{S_h \alpha_h \eta_{0,h}}{\rho_h C p_h A_h L}(T_h - T_w) \tag{25}$$

Table 2. Hot passage dynamic mathematical model.

Mass conservation equation
$$\frac{\partial \rho_c}{\partial t} = \frac{\partial(\rho_c u_c)}{\partial x} \tag{26}$$
Momentum conservation equation
$$\frac{\partial(\rho_c u_c)}{\partial t} = \frac{\partial(\rho_c u_c^2)}{\partial x} + \frac{\partial P_c}{\partial x} - \frac{U_c \sigma_c}{A_c} \tag{27}$$
Energy conservation equation
$$\frac{\partial T_c}{\partial t} = u_c \frac{\partial T_c}{\partial x} - \frac{S_c \alpha_c \eta_{0,c}}{\rho_c C p_c A_c L}(T_c - T_w) + \frac{1}{\rho_c C p_c Y_c} \sum_{k\in\{(I),(II),(III)\}} (-\Delta H)_k R_k \tag{28}$$

Table 3. Cold passage dynamic mathematical model.

For the solid structures, such as the fins and the separators, the temperature is considered to be uniform at the same cross-section. The energy conservation equation is written as:

$$\frac{\partial T_w}{\partial t} = K \frac{\partial^2 T_w}{\partial x^2} + \frac{\alpha_h S_h \eta_{0,h}}{M_w C p_w}(T_w - T_h) + \frac{\alpha_c S_c \eta_{0,c}}{M_w C p_w}(T_w - T_c) \tag{29}$$

The heat conductivity coefficient is $K = L\lambda_w A_w / M_w Cp_w$, the cross area of solid structure is $A_w = 2Wt + n_h(X_h + Y_h + t_h)t_h + n_c(X_c + Y_c + t_c)t_c$, and the mass is $M_w = \rho_w A_w L$.

The control equations of the heat exchange reformer are strongly coupled. In addition to the partial differential equations presented above, two perfect state equations $P=f(\rho, T)$ for the hot and cold passages are also needed in order to compose a close equation set.

4. Simulation modelling and conditions

4.1 Volume-resistance characteristic model

In general, nonlinear partial differential equations are treated numerically. However, stability is one crucial factor when using a difference algorithm. In addition, the time step for the difference algorithm is usually very short, so the numerical process is very time consuming [4].

In order to avoid the coupled iteration between the flow rate and pressure, the volume-resistance characteristic modeling technique [4, 22] is introduced into the heat exchange reformer. This modeling technique is based on the lumped-distributed parameter method, which can obtain a set of ordinary differential equations from partial differential equations.

The volume-resistance characteristic model is listed in Table 4 in detail.

Hot passage

$$\frac{dP_{h,1}}{dt} = \frac{RT_{h,1}}{M_h A_h}\frac{G_{h,1} - G_{h,2}}{dx} \tag{30}$$

$$\frac{dG_{h,2}}{dt} = A_h \frac{P_{h,1} - P_{h,2}}{dx} - U_h \sigma_{h,2} \tag{31}$$

$$\frac{dT_{h,2}}{dt} = -\frac{G_{h,2}}{A_h \rho_{h,2}}\frac{T_{h,1} - T_{h,2}}{dx} - \frac{S_h \alpha_{h,2}}{\rho_{h,2} Cp_{h,2} A_h L}(T_{h,2} - T_{w,2}) \tag{32}$$

Cold passage

$$\frac{dC_{c,i,2}}{dt} = -\frac{u_{c,2}C_{c,i,2} - u_{c,1}C_{c,i,1}}{dx} + \sum_{k\in\{(I),(II),(III)\}} v_{i,k}R_{k,2}\frac{1}{Y_c} \quad i \in \{CH_4, H_2, CO, CO_2, H_2O\} \tag{33}$$

$$\frac{dP_{c,2}}{dt} = \frac{RT_{c,2}}{M_c A_c}\frac{G_{c,2} - G_{c,1}}{dx} \tag{34}$$

$$\frac{dG_{c,1}}{dt} = A_c \frac{P_{c,2} - P_{c,1}}{dx} - U_c \sigma_{c,1} \tag{35}$$

$$\frac{dT_{c,1}}{dt} = \frac{G_{c,1}}{A_c \rho_{c,1}}\frac{T_{c,1} - T_{c,2}}{dx} - \frac{S_c \alpha_{c,1}}{\rho_{c,1} Cp_{c,1} A_c L}(T_{c,1} - T_{w,1}) + \frac{1}{\rho_{c,1} Cp_{c,1} Y_c}\sum_{k\in\{(I),(II),(III)\}} (-\Delta H)_{k,1} R_{k,1} \tag{36}$$

Solid structure

$$\frac{\mathrm{d}T_{\mathrm{w},2}}{\mathrm{d}t} = K_x \frac{T_{\mathrm{w},3} - 2T_{\mathrm{w},2} + T_{\mathrm{w},1}}{(\mathrm{dx})^2} - \frac{\alpha_{\mathrm{h},2} S_{\mathrm{h}}}{M_{\mathrm{w}} C p_{\mathrm{w}}} (T_{\mathrm{h},2} - T_{\mathrm{w},2}) - \frac{\alpha_{\mathrm{c},2} S_{\mathrm{c}}}{M_{\mathrm{w}} C p_{\mathrm{w}}} (T_{\mathrm{c},2} - T_{\mathrm{w},2}) \quad (37)$$

Table 4. Heat exchange reformer volume-resistance characteristic model.

4.2 Simulation conditions

In addition to the configuration and geometry parameters of the heat exchange reformer, as shown in Table 5, and fluid properties calculated at the local position, some boundary conditions were also required to carry out the simulation. These included inlet flow rate, fluid composition, and the inlet temperature and outlet pressure of both the hot and cold streams (Table 6).

System geometry parameters	
Length	1 m
Width	0.5 m
Height	0.532 m
Hot passage	
Width	4.5E-3 m
Height	6.5E-3 m
Offset strip fin length	0.05m
Fin thickness	3.0E-3 m
Cold passage	
Width	4.5E-3 m
Height	5.0E-3 m
Offset strip fin length	0.05m
Fin thickness	5.0E-3 m
Separator	
Thickness	1.0E-3 m
Solid structure properties (SiC ceramic [27-29])	
Density	3100 kgm^{-3}
Heat capacity	0.640 $kJkg^{-1}K^{-1}$
Thermal conductivity	0.080 $kJm^{-1}s^{-1}K^{-1}$
Catalyst properties	
thickness	5.0E-5 m
Density	2355 kgm^{-3}
Catalyst reduced activity	0.003

Table 5. Geometry and properties parameters of heat exchange reformer.

Simulation conditions	
Cold fuel	
Inlet mass flow rate (kgs^{-1})	0.06
Inlet temperature (K)	898
Fluid molar fraction	$0.25CH_4$,$0.75H_2O$ (STC=3:1)
Outlet pressure (Pa)	1.0E+5
Hot waste gas	
Inlet mass flow rate (kgs^{-1})	0.4
Inlet temperature (K)	1200
Fluid molar fraction	$0.1CO_2$,$0.2H_2O$,$0.1O_2$,$0.6N_2$
Outlet pressure (Pa)	1.0E+5

Table 6. Key simulation parameters under the basic condition.

At the same time, some simplifying conditions are used to solve the equations; for example, the heat flux of both the solid structure at inlet and outlet are considered to be zero. As a result, contrasted to the centre difference algorithm in the middle of the solid structure, the difference algorithms for both the front and end modules are treated independently.

5. Results and discussions

In this section, due to the high cost of the complicated experiments, only simulation studies are employed on a counter-flow type heat exchange reformer. Section 5.1 provides the distributed characteristics of some important parameters, such as fuel species, temperature, and fluid properties (pressure, density, velocity, heat capacity, thermal conductivity and dynamic viscosity), under steady state conditions. Section 5.2 compares and analyzes the results under different input parameter conditions, such as steam to carbon ratio, catalyst reduced activity, and operating outlet pressure. In Section 5.3, the dynamic behaviours of the compact heat exchanger reformer are investigated.

5.1 Steady state result analysis

For the rated condition, some related parameters are presented in Table 6, such as inlet temperature, mass flow rate, molar fraction, and outlet pressure.

Fig. 4 presents the fuel molar fraction along the heat exchange reformer length. The flow direction in the fuel channel is from 1.0 to 0 in the figures, so all the parameters in the fuel channel should be understood to proceed from 1.0 to 0. At the cold fuel passage inlet, the fluid only contains methane and water. The steam reforming reaction takes place on the surface of the catalyst along the flow direction. Therefore, the methane is gradually consumed. The methane and water concentration decreases along the flow direction. The concentration of produced hydrogen gradually increases. The methane steam reforming reaction has two simultaneous effects. The carbon monoxide molar fraction increases and the carbon dioxide molar fraction increases along the flow direction. At the exit, the flow composition is 4.24% of CH_4, 45.35% of H_2, 10.00% of CO, 3.84% of CO_2, and 36.57% of H_2O.

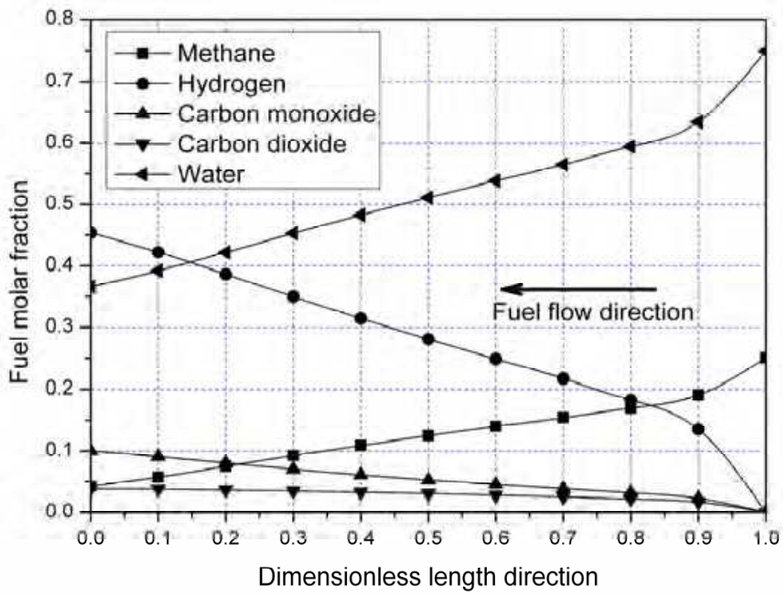

Fig. 4. Fuel molar fraction along the heat exchange reformer length.

The temperature profiles of the cold stream, hot stream, and solid structure along the heat exchange reformer length are presented in Fig. 5. Because of the high endothermic methane reforming reaction, the cold fuel temperature decreases a little at the entrance. Then, the cold fuel temperature increases along its flow direction due to the heat transfer from hot gas. The temperatures of the hot gas stream and the solid structure decrease along the heat exchange reformer length. It should be noted that the temperature curve is just the line between measured points, so it can't indicate the trend at both ends.

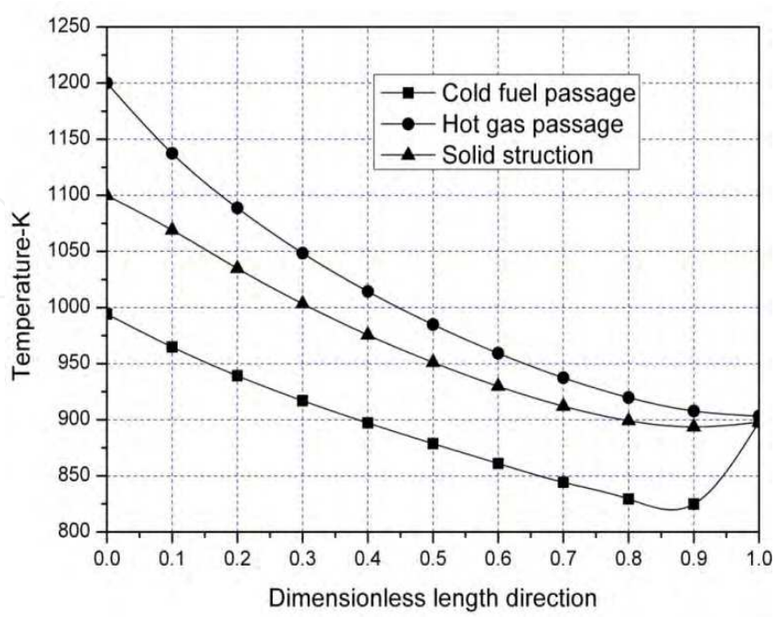

Fig. 5. Temperature distribution along the heat exchange reformer length.

The pressure profiles in the cold fuel and hot gas passages are illustrated in Fig. 6. Owing to the friction of the passage, the pressure loss is about 0.08% in the cold fuel passage, and about 4.23% in the hot gas passage. The primary reason that the pressure loss is greater in the hot gas passage is that the mass flow rate in the hot gas passage is larger than that in the cold passage. Of course, the geometrical configuration is a key factor as well.

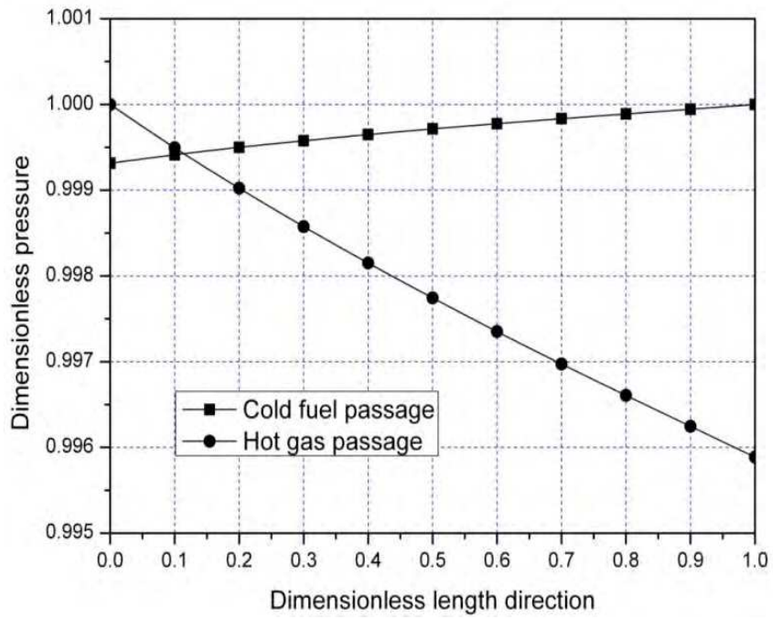

Fig. 6. Pressure distribution along the heat exchange reformer length.

The dimensionless fluid properties (such as: density, velocity, heat capacity, thermal conductivity, and dynamic viscosity) of the cold fuel and hot gas along the heat exchange reformer are illustrated in Fig. 7 and Fig. 8, respectively. The dimensionless properties are defined as the ratio of local values and corresponding inlet values, which can be calculated by the inlet conditions in the methods depicted in the reference [23]. Examples of this include situations where: the density is based on the gas state equation; the velocity is calculated by the mass flow rate, density and the channel cross area; the heat capacity of the multi-component gas mixture is related to the single component heat capacity and the corresponding molar fraction; the dynamic viscosity of the multi-component gas mixture is based on the Reichenberg's expression; the thermal conductivity of multi-component gas mixtures is based on Wassiljewa's expression and the Mason & Saxena modification.

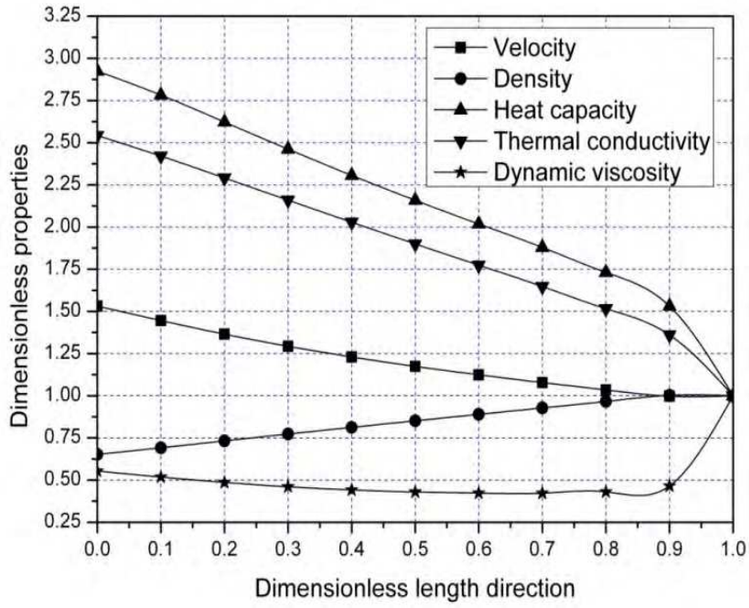

Fig. 7. Cold fuel properties along the heat exchange reformer length.

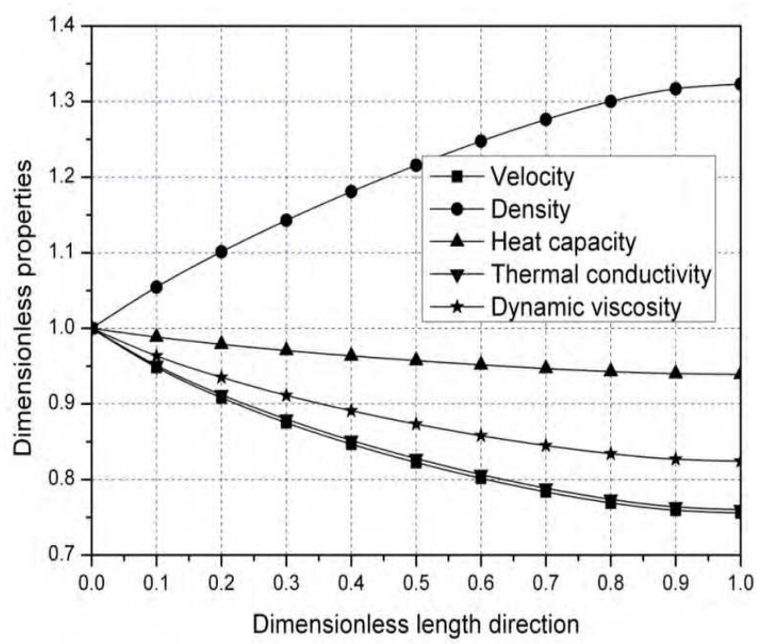

Fig. 8. Hot gas properties along the heat exchange reformer length.

The density is related to the pressure and the temperature, which are decided by the gas state equation $P = \rho RT$. In the cold fuel passage, the temperature increases and the pressure decreases, so the density decreases along the flow direction while, in the hot gas passage, both the pressure and the temperature decrease. The ratio of pressure and temperature along the passage is increased, so the density of the hot gas increases along the flow direction.

Two primary factors that affect the velocity are the mass flow rate and the density. Here, the mass flow rate is constant, and the velocity is mainly determined by the density. That is to say, the velocity increases in the cold fuel passage and decreases in the hot gas passage, following the trend of the density.

Specific heat capacity, thermal conductivity, and dynamic viscosity are primarily influenced by the temperature and the gas composition. This has been discussed by Todd and Young [24] and Lijin WANG [22] for high temperature SOFCs.

5.2 Analysis of the influence of some parameters

In this section, some key parameters that affect the heat exchange reformer performance are investigated, such as the steam to carbon ratio (STC), catalyst reduced activity (CRA), and passage operating pressure.

5.2.1 Steam to carbon ratio

In general, the STC must be greater than 2.0 to avoid carbon coking in the fuel lines, reformer, and fuel cell stack [25]. The effect of different STCs on the heat exchange reformer is presented in Fig. 9 and Fig. 10.

Fig. 9 presents effect of STC on the methane and hydrogen distribution along the heat exchange reformer. In the internal reforming high temperature fuel cell, the endothermic reforming reaction will cause a great temperature gradient, which could decrease the life of the fuel cell stack due to excessive thermal stress. Therefore, too much remaining methane would be no good for the steady operation of the high temperature fuel cell. With the STC changing from 2:1 to 4:1, less methane remains at the exit (Fig. 9 (a)), while the hydrogen molar fraction at the exit is almost the same as at the entrance (Fig. 9 (b)). Therefore, a suitable and acceptable STC is essential for the internal reformation of high temperature fuel cells.

The temperature distribution of cold fuel and hot gas is illustrated in Fig. 10. When the STC changes from 2:1 to 4:1, less methane is provided at the inlet, and less heat is needed for the steam reforming reaction. Meanwhile, a higher STC will result in a higher rate of the exothermic water gas-shift reaction, so the temperature curves of both the cold and hot stream are higher.

5.2.2 Catalyst reduced activity

The CRA is defined as the ratio between the activity of the catalyst in use and that of a conventional Ni catalyst (Xu and Froment, [19]) at typical feed conditions (temperature, pressure, and composition) [26]. The CRA is the key factor in determining the reforming reaction rate. For the rated case, the CRA is defined as 0.003 [7] in Table 5. Fig. 11 and Fig. 12 present the effect of the CRA on the performance of the heat exchange reformer.

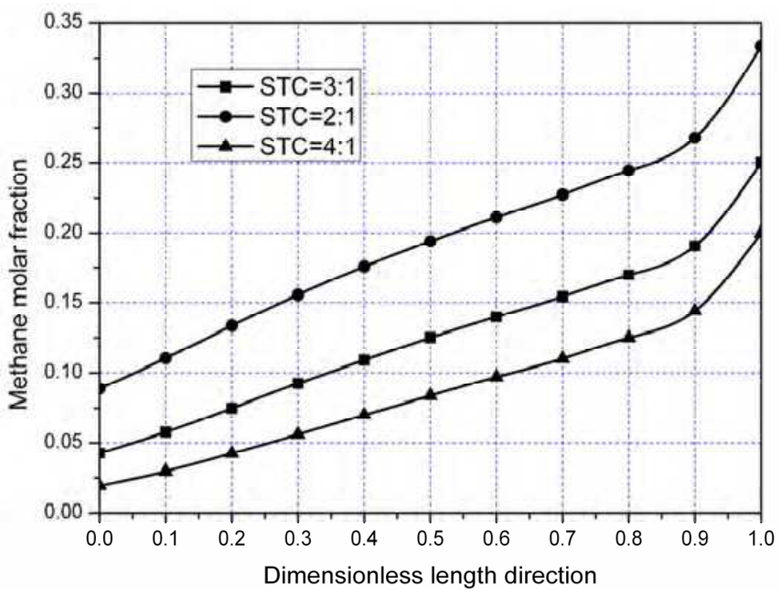

(a)

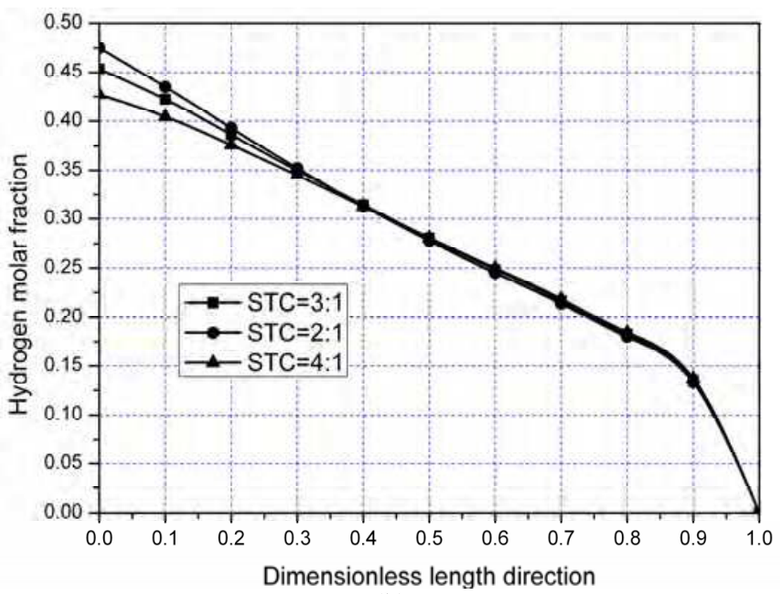

(b)

Fig. 9. STC effect on the methane (a) and hydrogen (b) molar fraction distributions.

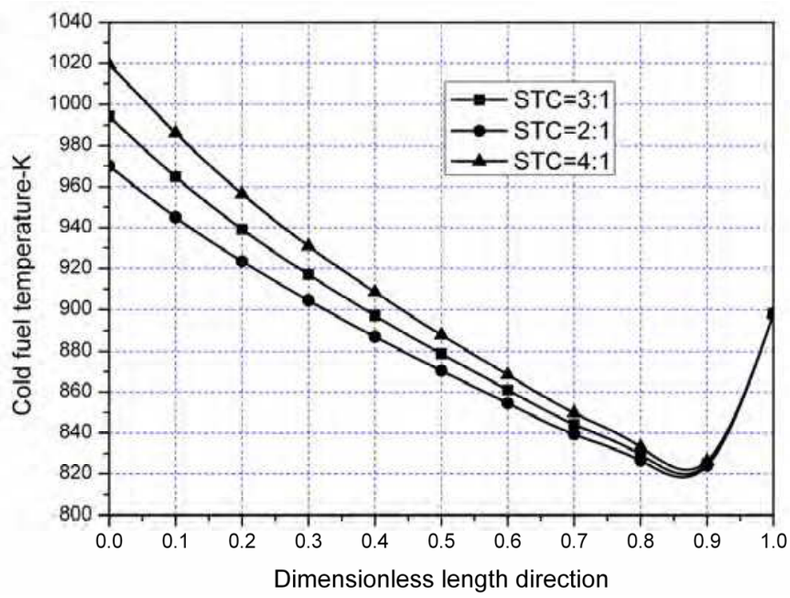

(a)

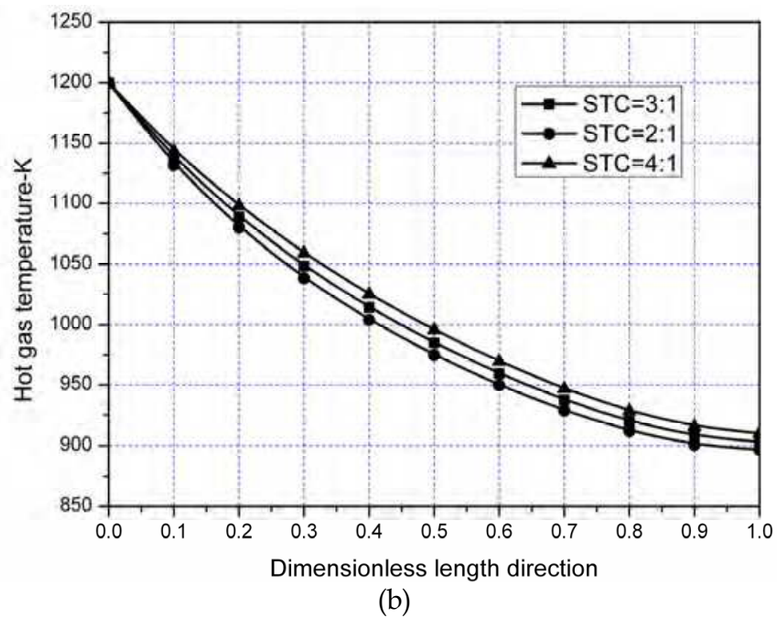

(b)

Fig. 10. STC effect on the cold fuel (a) and hot gas (b) temperature distributions.

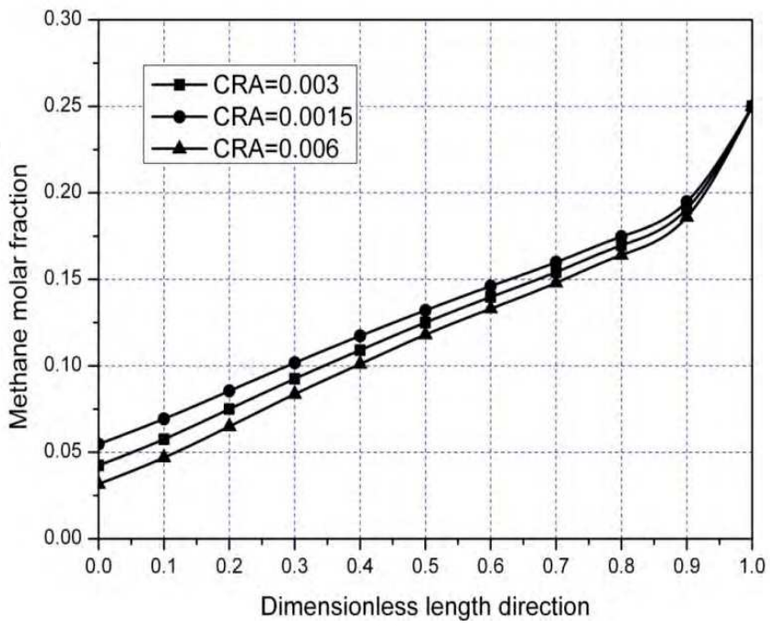

(a)

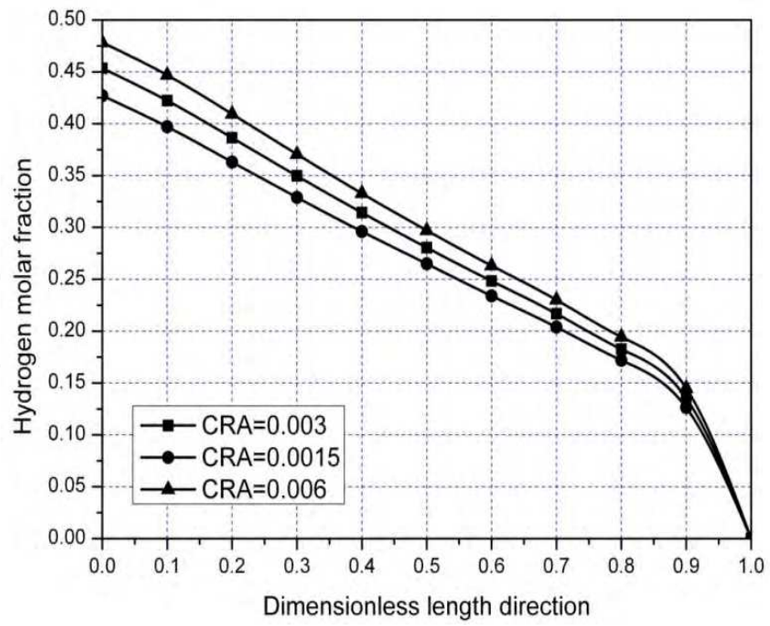

(b)

Fig. 11. CRA effect on the methane (a) and hydrogen (b) molar fraction distributions.

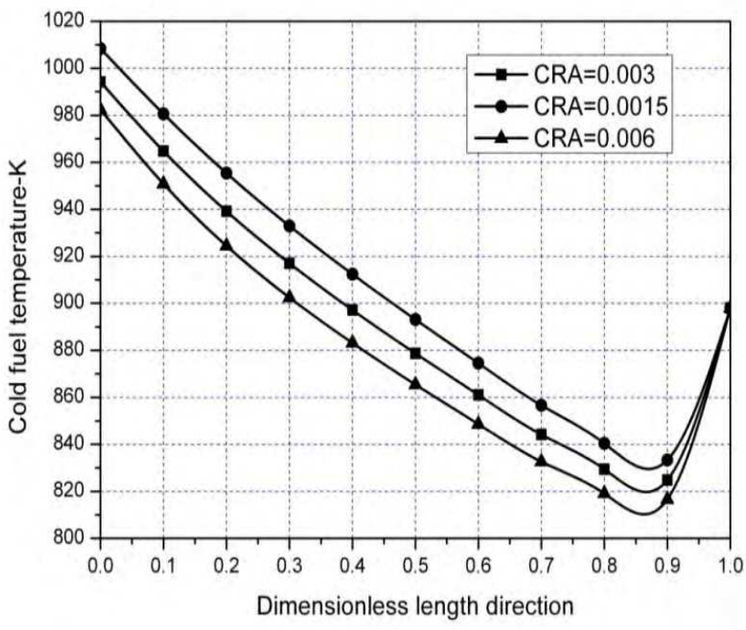

(a)

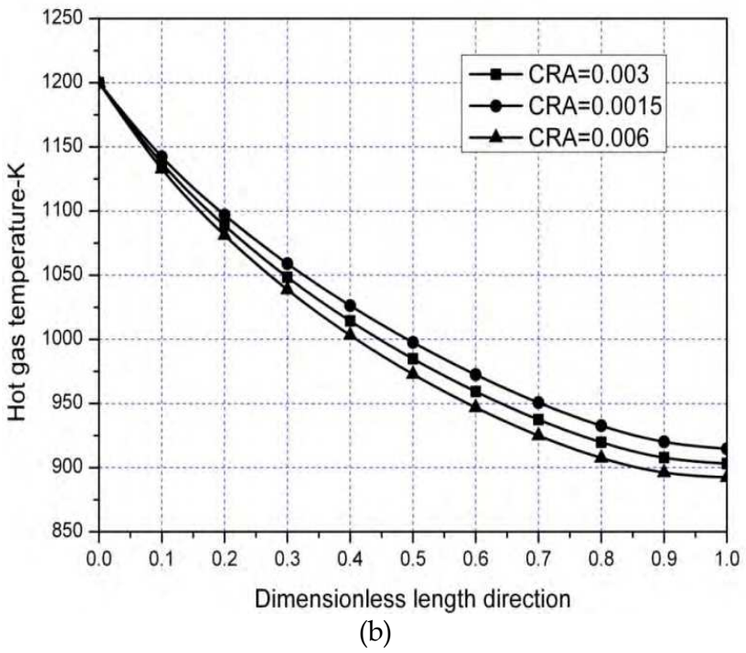

(b)

Fig. 12. CRA effect on the cold fuel (a) and hot gas (b) temperature distributions.

The influence on the methane and hydrogen molar fraction distribution along the heat exchange reformer is shown in Fig. 11. When the CRA changes from 0.0015 to 0.006, the rate of the methane reforming reaction increases, so more methane is consumed (Fig. 11 (a)) and more hydrogen is produced (Fig. 11 (b)). More heat is needed to satisfy the requirements of the high endothermic reaction, so the temperature curves of both the cold and hot stream are lower (Fig. 12).

5.2.3 Passage operating pressure

The passage pressure often changes with the operation condition, even during malfunctions or damage. The effect of the cold passage outlet pressure on the heat exchange reformer is investigated in this section and illustrated in Fig. 13 and Fig. 14.

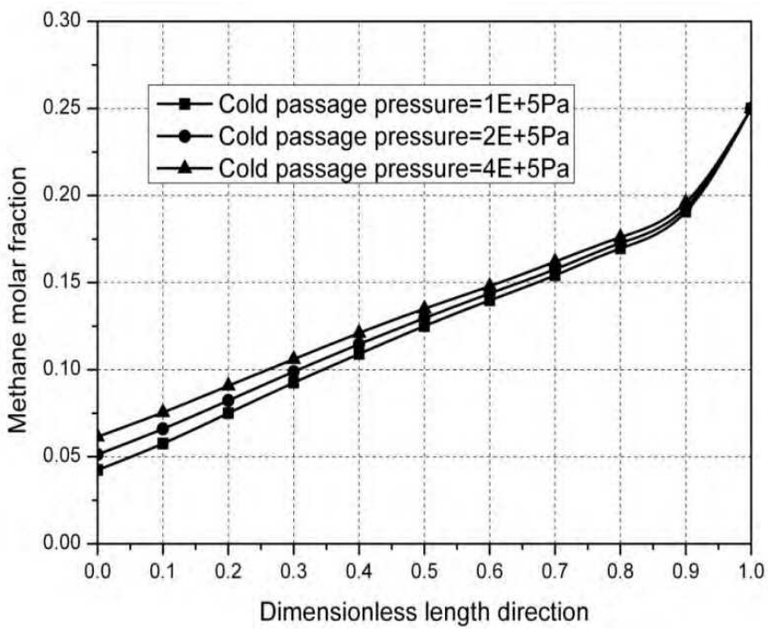

(a)

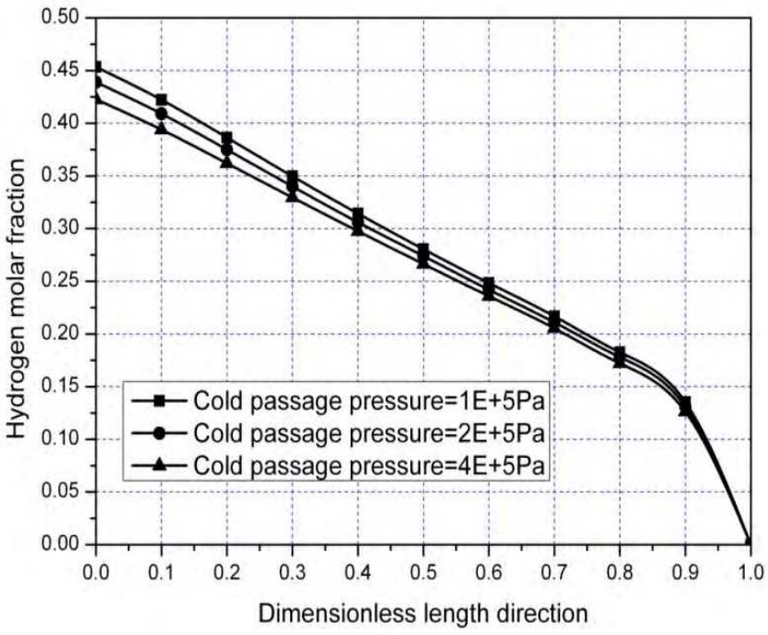

(b)

Fig. 13. Cold passage outlet pressure effect on the methane (a) and hydrogen (b) molar fraction distributions.

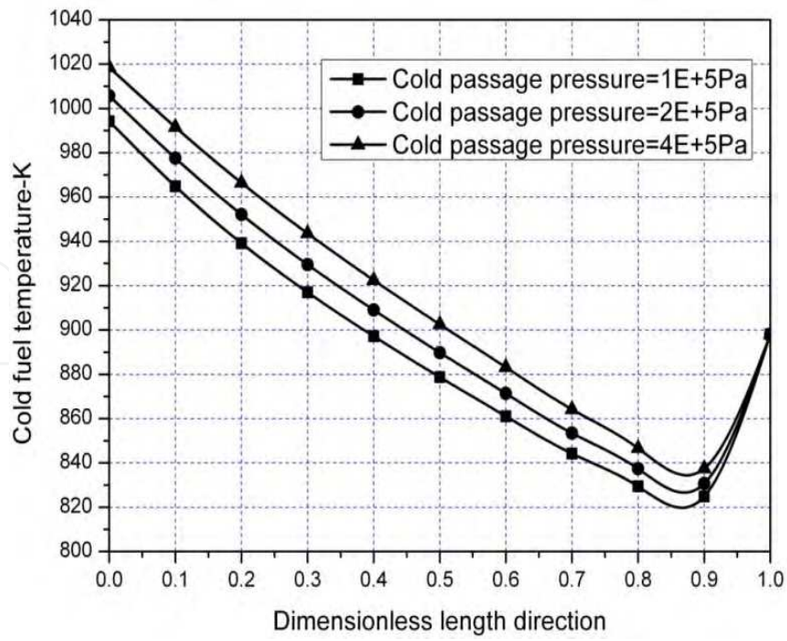

(a)

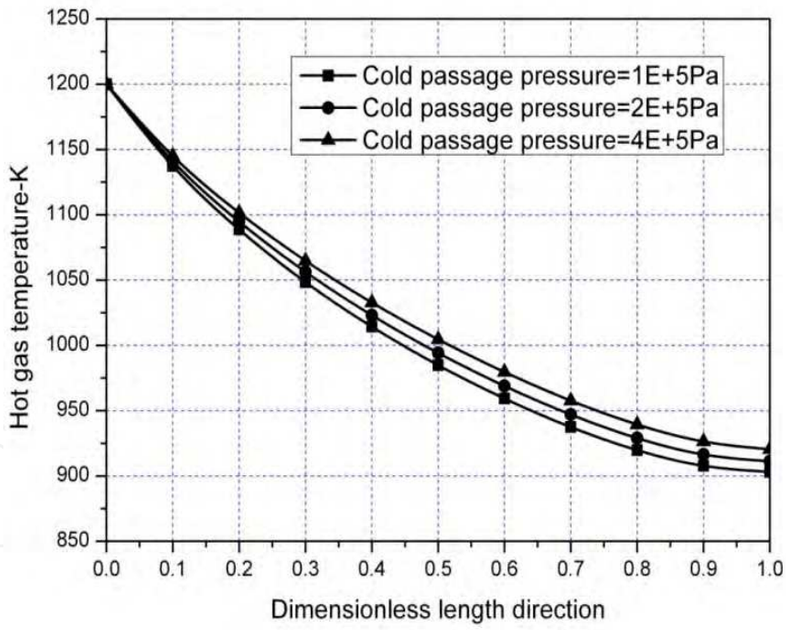

(b)

Fig. 14. Cold passage outlet pressure effect on the cold fuel (a) and hot gas (b) temperature distributions.

The cold passage outlet pressure has little influence on the heat exchange reformer performance. When the passage pressure is elevated from 1E+5Pa to 4E+5Pa, less methane is consumed, less hydrogen is produced (Fig. 13), and less heat is needed for the methane steam reforming reaction, so the cold fuel and hot gas temperatures are higher (Fig. 14).

5.3 Dynamic simulation result

In this section, the transient behaviours of the compact heat exchange reformer are investigated. Several step-change input parameters (such as inlet mass flow rate and inlet temperature of both the cold and hot stream) are imposed when the device has been operated for 500s.

Fig. 15 illustrates the dynamic response of the temperatures at the cold and hot passage exits, when the cold fuel mass flow rate has a step increase of 10%. The cold passage exit temperature has a sudden decrease at the initial period due to the step input. Then, because of the great thermal inertia of the solid structure, the temperature decreases gradually. Therefore, the temperature at the cold passage exit decreases. Owing to a greater cold fuel mass flow rate, more heat is provided from the hot side, so the temperature at the hot passage exit has a gradual decrease.

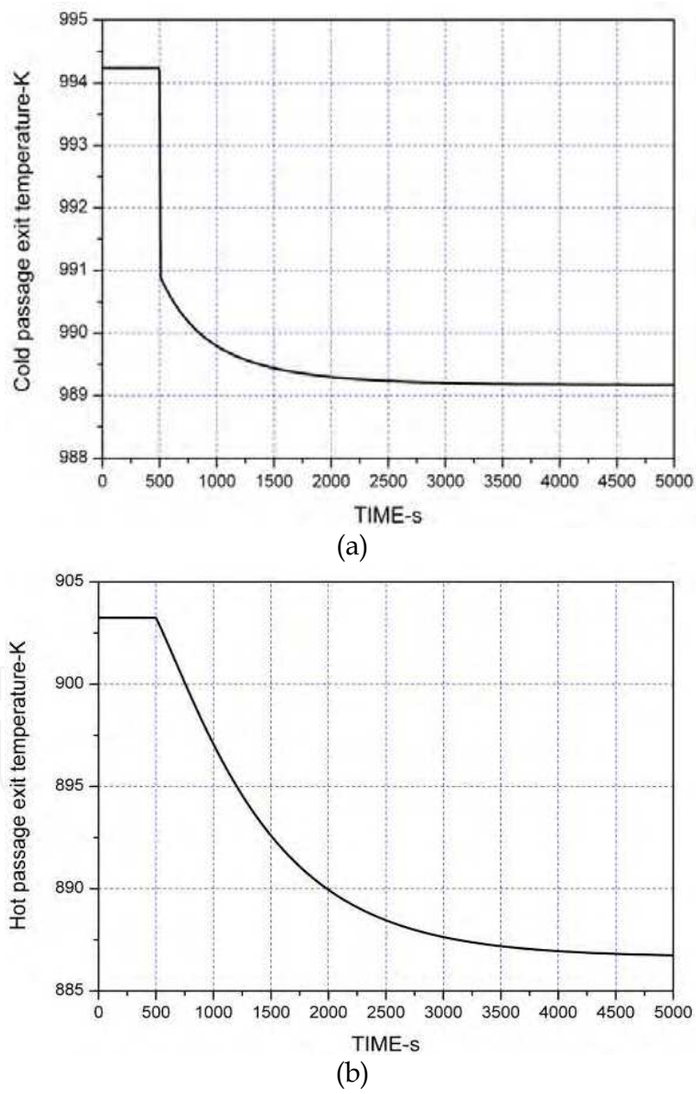

Fig. 15. Dynamic response of the temperatures at the Cold (a) and hot (b) passage exits when cold fuel mass flow rate up by 10%.

Fig. 16 shows the dynamic effect on methane, hydrogen, and the water molar fraction distribution when the cold fuel mass flow rate has a step increase of 10%. The methane and water molar fraction increase a little, while the hydrogen decreases a little. It can be shown that the molar fraction has a little change when the cold fuel inlet mass flow rate changes.

Fig. 17 presents the dynamic response of the cold fuel and hot gas temperatures when the hot gas inlet temperature decreases to 1100K from 1200K. The temperature at the cold passage exit is influenced by the thermal capacity of the solid structure, and decreases gradually. Owing to the decrease of the inlet temperature, the temperature at the hot gas passage exit also undergoes a decrease (Fig. 17 (b)). When the temperature of the cold stream decreases, the rate of the steam reforming reaction will be slower. Therefore, less fuel is reformed, which can be shown from the methane molar fraction distribution in Fig. 18 (a); less hydrogen is produced (Fig. 18 (b)) and more water remains (Fig. 18 (c)).

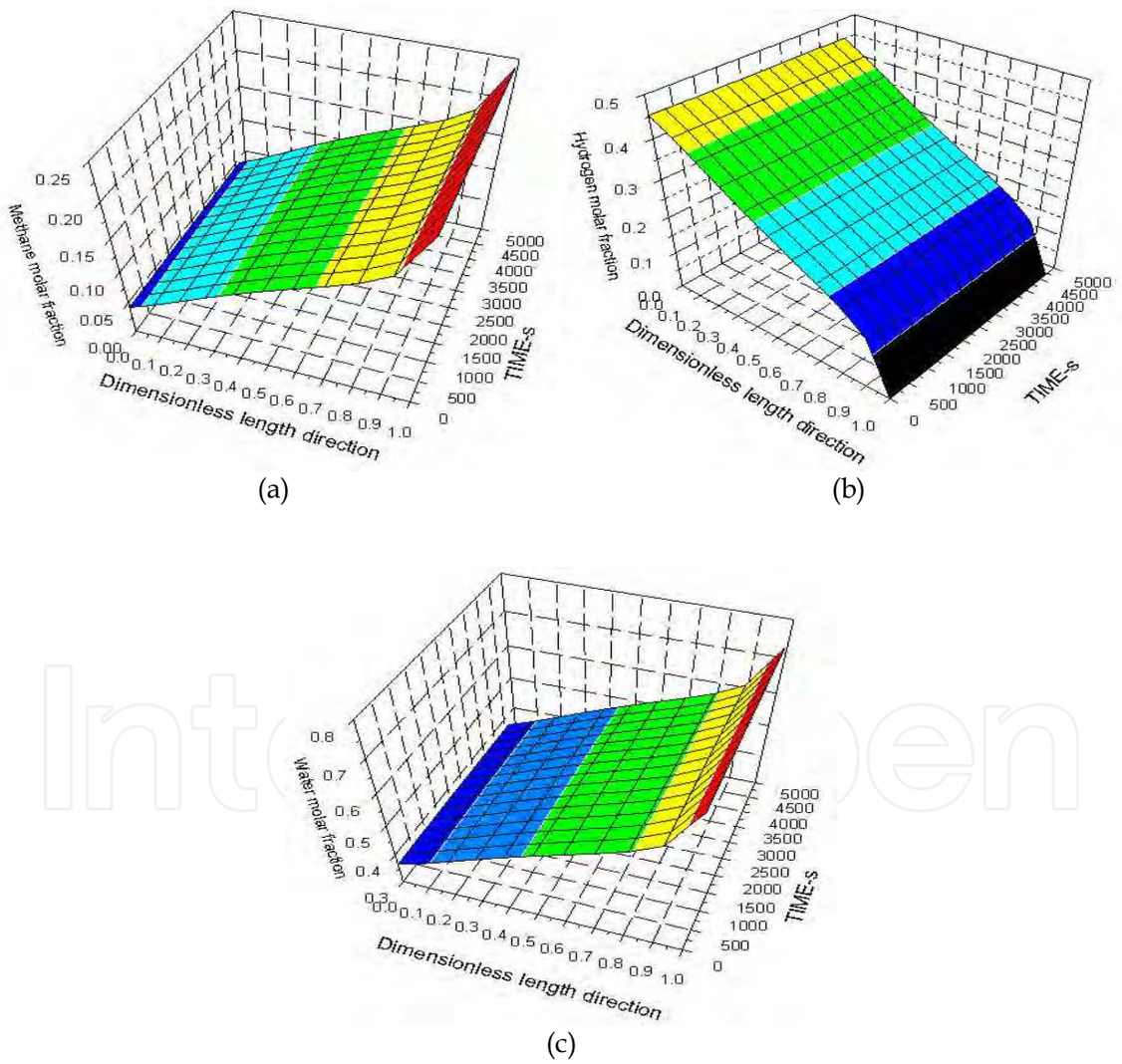

Fig. 16. Dynamic response of methane (a), hydrogen (b) and water (c) distributions when cold fuel mass flow rate up by 10%.

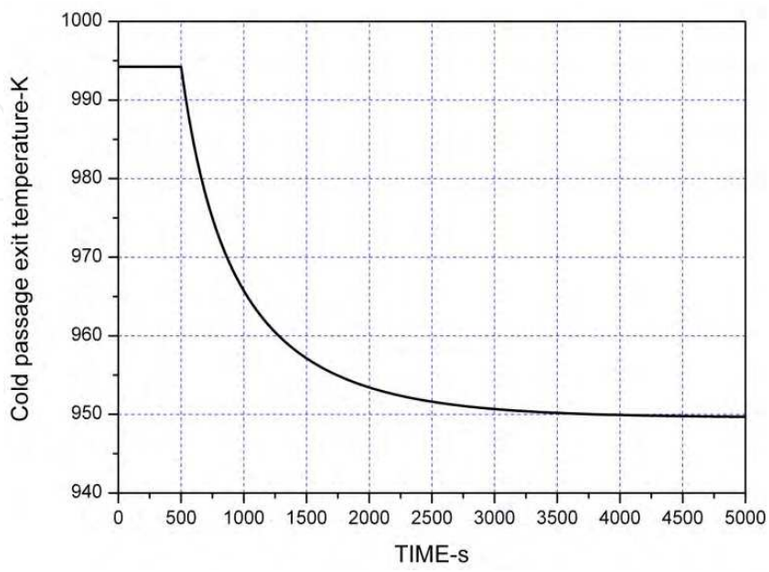

(a)

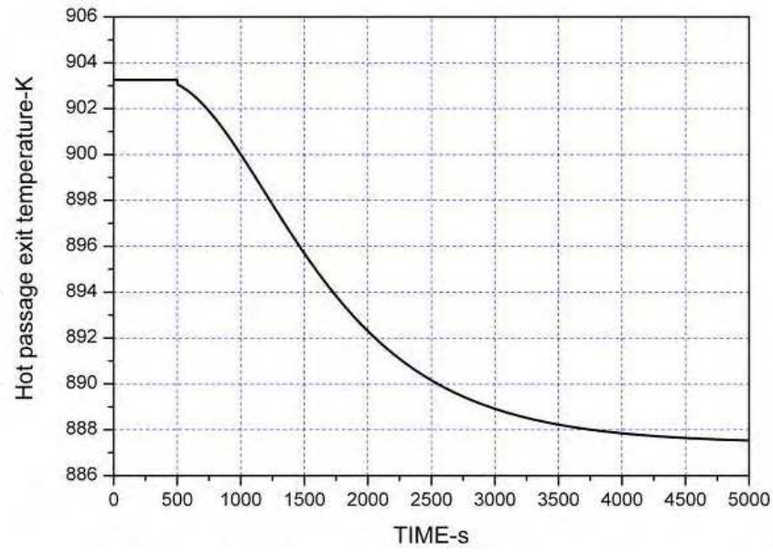

(b)

Fig. 17. Dynamic response of the temperatures at the cold (a) and hot (b) passage exits when the hot inlet temperature down to 1100K.

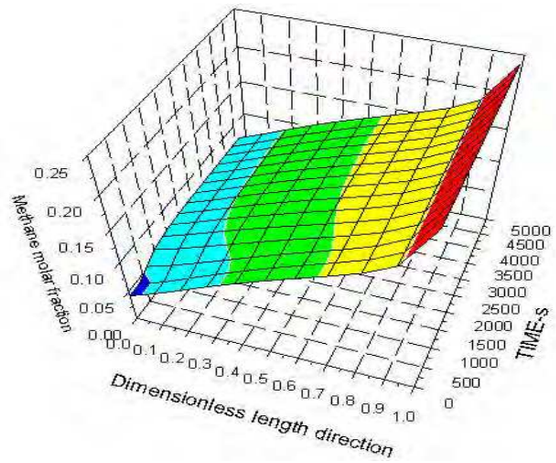

(a)

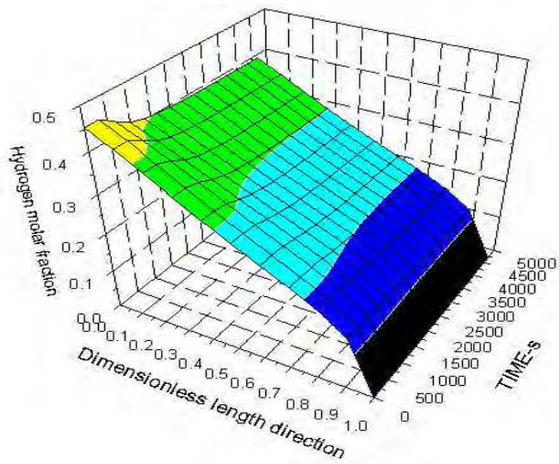

(b)

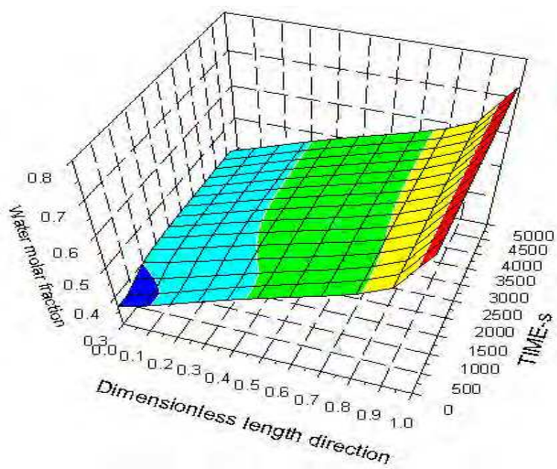

(c)

Fig. 18. Dynamic response of methane (a), hydrogen (b) and water (c) distributions when the hot inlet temperature down to 1100K.

Based on all the dynamic performance figures from Fig. 15 to Fig. 18, the inertial delay time of this kind of heat exchange reformer is about 3000s. Such a substantial thermal inertia can seriously influence the whole fuel cell hybrid system transient performance and the design of the control system.

6. Conclusions

A compact heat exchange reformer for high temperature fuel cell systems is presented in this paper. Based on the volume-resistance characteristic modeling technique, the distributed-lumped parameter method, and the modular modeling idea, a simulation model that is suited for quick and real time simulations is completed. The model can predict the key distribution characteristic parameters and the influence of some factors, such as the steam to carbon ratio, catalyst reduced activity, and passage pressure. The dynamic results indicate that this kind of heat exchange reformer has a great thermal inertia.

Both the model and modeling method will be useful and valuable for other heat exchange reformer designs and optimization; it can also provide a reference for the design of the control system in the future.

7. Acknowledgement

Financial support from the National Natural Science Foundation of China (NSFC) under the contract no. 50676061 and Shanghai Key Research Program from Science and Technology Committee of Shanghai Municipal under the contract No. 09DZ1200701 and 09DZ1200702 is gratefully acknowledged

8. Nomenclature

A	area (m^2)
C	molar concentration ($molm^{-3}$)
C_p	specific heat capacity ($kJkg^{-1}K^{-1}$)
D_h	hydraulic diameter (m)
DEN	parameter used in Table 1
f	fanning friction factor
G	mass flow rate (kgs^{-1})
G_m	mass velocity ($kgm^{-2}s^{-1}$)
J	Colburn factor
K	parameter used in Table 1
k	parameters used in Table 1, or geometry parameter used in formula (8) (m)
L	heat exchanger length (m)
l	offset strip fin length (m)
M	molecular weight ($kgmol^{-1}$)
n	number
p	partial pressure of component i in the cold fuel passage (Pa)
P	pressure (Pa)
Pr	Prandtl number
R	gas constant ($Jmol^{-1}K^{-1}$)
Re	Reynolds number

S passage heat transfer surface (m)
St Stanton number
T temperature (K)
t fin or plate thickness (m), time (s)
U wet perimeter (m)
u velocity (ms^{-1})
W whole heat exchanger width (m)
X passage width (m)
Y passage height (m)

Greek letters

α convective heat transfer coefficient ($kJm^{-1}s^{-1}K^{-1}$) or dimensionless geometry parameter used in formula (13) and (15)
δ dimensionless geometry parameter used in formula (13) and (15)
γ dimensionless geometry parameter used in formula (13) and (15)
ρ density (kgm^{-3})
η fin efficiency
σ friction resistance
μ dynamic viscosity (Pa.s)
λ thermal conductivity ($kJm^{-1}s^{-1}K^{-1}$)
ΔH, ΔH^0 enthalpy change and enthalpy change at the standard state ($kJmol^{-1}$)
ΔP pressure loss (Pa)

Subscripts

c cold side
f fin
h hot side
i fuel component
w solid fin structure
(I) steam reforming reaction
(II) gas shifting reaction
(III) CO_2 direct reforming reaction

9. References

[1] EG&G Technical Services Inc, M. (2004). *Fuel Cell Handbook* (seventh edition), U. S. Department of Energy Office of Fossil Energy National Energy Technology Laboratory. New York, USA.

[2] Larminie, J. & Dicks, A., M. (2003). *Fuel Cell Systems Explained* (Second edition), John Wiley & Sons Ltd, England.

[3] Dicks, A.L., J. (1998). Advances in catalysts for internal reforming in high temperature fuel cells, *Journal of Power Sources*, 71(1998) pp.111-122.

[4] Zhang, H.S.; Weng, S.L. & Su M. (2005). Dynamic modeling and simulation of distributed parameter heat exchanger, *Proceedings of ASME TURBO EXPO* 2005-68293, Nevada, USA, June 14-17, 2005.

[5] Shah, R. K. & Webb, R. L., M. (1983). *Compact and enhanced heat exchangers, Heat Exchangers: Theory and Practice*, Hemisphere, Washington, DC.

[6] Zanfir, M. & Gavriilidis, A., J.(2003). Catalytic combustion assisted methane steam reforming in a catalytic plate reactor, *Chemical Engineering Science*, 58(2003) pp. 3947-3960.

[7] Lim, L.T.; Chadwich, D. & Kershenbaum, L., J.(2005). Achieving autothermal operation in internally reformed solid oxide fuel cells: Simulation studies, *Ind. Eng. Chem. Res.* 44 (2005) pp. 9609-9618.

[8] Plate-fin heat-exchange reformer with highly dispersed catalyst, *Fuel Cells Bulletin*, 4(37) (2001) 16

[9] Wegeng, R.S.; Pederson, L.R.; TeGrotenhuis, W.E. & Whyatt, G.A., Compact fuel processors for fuel cell powered automobiles based on microchannel technology. *Fuel Cells Bulletin*, 3(28) (2001) 8-13.

[10] Patil, A.S.; Dubois, T.G.; Sifer, N. & Bostic, E., J. (2004). Portable fuel cell systems for America's army: technology transition to the field, *Journal of Power Sources* 136(2004) pp. 220-225.

[11] Tonkovich, A.Y.; Perry, S.; Wang, Y.; Qiu, D.; LaPlante, T. & Rogers, W.A., J. (2004). Microchannel process technology for compact methane steam reforming. *Chemical Engineering Science* 59(2004) pp. 4819-4824.

[12] Ryi, S.K.; Park, J.S.; Choi, S.H.; Cho, S.H. & Kim, S.H., J. (2005).Novel micro fuel processor for PEMFCs with heat generation by catalytic combustion. *Chemical Engineering Journal* 113(2005) pp. 47-53.

[13] Park, G.G.; Yim, S.D.; Yoon, Y.G.; Lee, W.Y.; Kim, C.S.; Seo, D.J. & Eguchi, K., J. (2005). Hydrogen production with integrated microchannel fuel processor for portable fuel cell systems. *Journal of Power Sources* 145(2005) pp. 702-706.

[14] Kays, W.M. & London, A.L., M. (1984). *Compact Heat Exchangers*, McGraw Hill, New York, Third Edition, 1984.

[15] ALPEMA, (2000) *The standards of the brazed Aluminum plate-fin heat exchanger manufactures' association*, Second Edition, 2000

[16] Hachemi, A., J. (1999). Experimental study of thermal performance of offset rectangular plate fin absorber-plates, *Renewable Energy* 17 (1999) pp.371-384.

[17] Manglik, R.M. & Bergles, A.E., J. (1995).Heat Transfer and Pressure Drop Correlations for the Rectangular Offset Strip Fin Compact Heat Exchanger, *Experimental Thermal and Fluid Science* 10 (1995) pp.171-180.

[18] Rosehnow, W.M., M. (1985). *Handbook of heat transfer applications*, 2nded, USA: McGraw-Hill; 1985.

[19] Xu, J. & Froment, G.F., J. (1989).Methane steam reforming, methanation and water gas shift: I Intrinsic kinetics, *AIChE* 35 (1989) pp.3929-3940

[20] Smith, J.M.; Van Ness, H.C. et.al, M. (2005). *Introduction to Chemical Engineering Thermodynamics 7th edition*, McGraw-Hill, New York, 2005, pp.140-141.

[21] Luo, X.; Guan, X. et.al, J. (2003). Dynamic behavior of one-dimensional flow multistream heat exchangers and their networks, *Int. J. Heat Mass Transfer* 46 (2003) 705-715.

[22] Wang, L.J.; Zhang, H.S. & Weng, S.L., J. (2008). Modeling and simulation of solid oxide fuel cell based on the volume-resistance characteristic modeling technique, *Journal of Power Sources* 177(2008) pp.579-589.

[23] Poling, B.E., Prausnnitz, J.M. et.al, M. (2000). *The Properties of Liquids & Gases*, 5th Edition, McGraw-Hill, New York, 2000.

[24] Todd, B. & Young, J.B., J. (2002). Thermodynamic and transport properties of gases for use in solid oxide fuel cell modeling, *Journal of Power Sources* 110 (2002) pp.186-200.

[25] Mueller, F.; Jabbari, F.; Gaynor, R. & Jacob, B., J. (2007). Novel solid oxide fuel cell system controller for rapid load following, *Journal of Power Sources* 172 (2007) pp.308-323.

[26] Aguiar, P.; Chadwick, D. & Kershenbaum, L., J. (2004). Effect of methane slippage on an indirect internal reforming solid oxide fuel cell, *Chemical Engineering Science* 59(2004) pp.87-97.

[27] Steen, M. & Ranzani, L., J. (2000). Potential of SiC as a heat exchanger material in combined cycle plant, *Ceramics International*, 26(2000) 849-854.

[28] Yasar, I., J. (2004). Finite element model for thermal analysis of ceramic heat exchanger tube under axial non-uniform convective heat transfer coefficient, *Materials and Design* 25(2004) 479-482.

[29] Akiyoshi, M.; Takagi, I.; Yano, T.; Akasaka, N. & Tachi, Y., J. (2006). Thermal conductivity of ceramics during irradiation, *Fusion Engineering and Design* 81 (2006) 321-325.

Heat Exchangers - Basics Design Applications
Edited by Dr. Jovan Mitrovic

ISBN 978-953-51-0278-6
Hard cover, 586 pages
Publisher InTech
Published online 09, March, 2012
Published in print edition March, 2012

Selecting and bringing together matter provided by specialists, this project offers comprehensive information on particular cases of heat exchangers. The selection was guided by actual and future demands of applied research and industry, mainly focusing on the efficient use and conversion energy in changing environment. Beside the questions of thermodynamic basics, the book addresses several important issues, such as conceptions, design, operations, fouling and cleaning of heat exchangers. It includes also storage of thermal energy and geothermal energy use, directly or by application of heat pumps. The contributions are thematically grouped in sections and the content of each section is introduced by summarising the main objectives of the encompassed chapters. The book is not necessarily intended to be an elementary source of the knowledge in the area it covers, but rather a mentor while pursuing detailed solutions of specific technical problems which face engineers and technicians engaged in research and development in the fields of heat transfer and heat exchangers.

INTECH
open science | open minds

InTech Europe
University Campus STeP Ri
Slavka Krautzeka 83/A
51000 Rijeka, Croatia
Phone: +385 (51) 770 447
Fax: +385 (51) 686 166
www.intechopen.com

InTech China
Unit 405, Office Block, Hotel Equatorial Shanghai
No.65, Yan An Road (West), Shanghai, 200040, China
中国上海市延安西路65号上海国际贵都大饭店办公楼405单元
Phone: +86-21-62489820
Fax: +86-21-62489821

IntechOpen